Journal of Magnetism and Magnetic Materials 549 (2022) 169043

Contents lists available at ScienceDirect

Journal of Magnetism and Magnetic Materials

journal homepage: www.elsevier.com/locate/jmmm

Creating and detecting a magnetic bimeron by magnetic force microscope probe

M.V. Sapozhnikov [a,b,*], D.A. Tatarskiy [a,b], V.L. Mironov [a]

[a] Institute for Physics of Microstructures RAS, GSP-105, Nizhny Novgorod, 603950, Russia
[b] N.I. Lobachevsky State University, Nizhny Novgorod, 603950, Russia

ARTICLE INFO

Keywords:
Magnetic topological states
Magnetic force microscopy
Micronagnetic simulations

ABSTRACT

A magnetic bimeron is a version of skyrmion, which is predicted for the in-plane magnetized thin films with interfacial Dzyaloshinskii-Moriya interaction. Here we theoretically investigate the possibility to create individual bimeron using stray field of magnetic force microscope (MFM) tip. We demonstrate that a local magnetization reversal of the film by localized MFM field in combination with an additional uniform perpendicular magnetic field enables the stable bimeron formation. The possibilities for detection of the bimeron by the methods of magnetic force microscopy, Lorentz transmission electron microscopy and magnetic resonance force spectroscopy are discussed.

The existence of topologically charged soliton solutions for the magnetization in ferromagnetic films was predicted back in the 1970 s [1,2]. Later they were predicted and found experimentally in non-centrosymmetric magnetic crystals[3,4] and since then have been referred to as "magnetic skyrmions". A new impulse was given to skyrmionic studies after it was shown that they could be stable in thin films of transition metals with perpendicular anisotropy even at room temperature[5]. This stability is due to the strong Dzyaloshinskii-Moriya interaction (DMI), which arises at the boundary of the ferromagnet (Co, Ni, Fe) and the metal with strong spin–orbit interaction (Pt, Ir)[6]. Such properties of a skyrmion as small size, topologically protected stability, and mobility under spin-polarized electric current make it possible to be exploited in spintronic racetrack memory and information processing devices[7–9]. Nevertheless, it has its drawbacks, for example, the transversal lateral drift of the skyrmion under the influence of the skyrmion Hall effect[10]. This is considered as a main problem upon utilizing magnetic skyrmions in racetrack devices. This raises the interest in other topological spin textures such as antiskyrmion, skyrmionium, biskyrmion, meron, antimeron, including bimeron[11].

Bimeron is the in-plane magnetized version of a skyrmion[12]. Indeed, it can be obtained from skyrmion by rotating the magnetization by 90° around the in-plane axis (Fig. 1 a,b). Evidently, such transformation conserves the topological charge of the system. Bimeron consists of a pair of merons[13] and is predicted for in-plane magnetized films. The second meron in the pair has the structure of antimeron with mutually reversed out-of-plane magnetized core (Fig. 1b). As the topological charge of the meron is q=+1/2, this gives q= + 1 for bimeron. So bimeron should demonstrate all the usual skyrmionic features noted above. Nevertheless, it has the specific difference. The bimeron is not characterized by an integer polarity of the background magnetization direction compared to the skyrmion. Bimeron can be rotated freely in the plane[14] in the case of isotropic film. As bimerons have reduced symmetry compared to skyrmions there is a specific current direction in relation to the in-plane magnetization for which bimerons move parallel to the current[11,15]. This makes bimerons more perspective for racetrack applications. The complexity of the experimental observation of bimerons is associated with a currently unresolved problem of the individual bimeron generation. The known unique experimental observations of a dense bimeron lattice in a chiral crystal $Co_8Zn_9Mn_3$ [16] or individual bimerons pinned by magnetic vortex particles[17] are not suitable solutions for the racetrack applications. The same obstacles have the highly pinned topologically trivial meron-antimeron pairs observed in Ta/Co/Pt trilayers[18].

In this work we theoretically investigate the possibility of a magnetic bimeron generation by an inhomogeneous field of a magnetic force microscope (MFM) tip. Such methods are well known for creating and manipulating magnetic skyrmion[19–21]. Previously it was shown that tip approaching the in-plane magnetized film forms the magnetization distribution like meron-antimeron pair[22] but with the same core directions. However this state annihilates when tip is moving away. Our

* Corresponding author.
E-mail address: msap@ipmras.ru (M.V. Sapozhnikov).

https://doi.org/10.1016/j.jmmm.2022.169043
Received 23 November 2021; Received in revised form 28 December 2021; Accepted 9 January 2022
Available online 12 January 2022

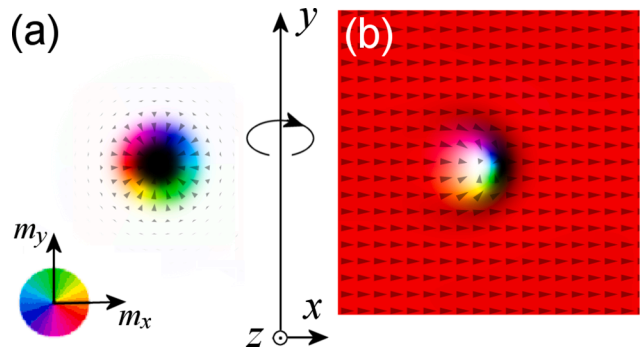

Fig. 1. (Color online). (a) The calculated magnetization distribution in the magnetic skyrmion. It can be transformed into magnetic bimeron (b) by magnetization rotation by 90° around y-axis. The size of the images corresponds to 768 × 768 nm^2.

idea is that the MFM tip approach to the film with strong interfacial DMI accompanied by application of additional external magnetic field will change the direction of the antimeron core introducing topological charge in the system. The appearing bimeron will be topologically stabilized by DMI after removing the MFM tip. The emerging bimeron can be detected directly with the MFM or with Lorentz transmission electron microscopy (LTEM). In addition, the presence of a bimeron should lead to a change in the ferromagnetic resonance

(FMR) spectrum of the system, which can be detected by magnetic resonance force microscope (MRFM)[23]. For this purpose, we calculate the expected MFM and LTEM Fresnel contrast distributions from bimeron and simulate the low frequency range of the FMR spectra connected with magnetization oscillations in the presence of bimeron.

We verify the suggested approach with micromagnetic simulations using the GPU-accelerated MuMax3 simulator[24] based on a numerical solution of the system of Landau-Lifshitz-Gilbert (LLG) equations for the magnetization of the system. The geometry of the simulated system is represented in Fig. 2. A square segment of a magnetic film has a size of 768 × 768 nm^2. Periodic boundary conditions in the plane of the system are used in order to simulate large film and avoid the film edge magnetostatic effects. The thickness of the film is 1 nm. The usual Co material parameters are used in the calculations[14]: saturation magnetization $M_S = 1300$ kA/m, exchange stiffness $J = 1.6 \times 10^{-11}$ J/m, damping parameter $\alpha = 0.01$. Effective anisotropy constant $K_{eff} = K - \mu_0 M_S^2/2$ is varied in the range–0.2 ÷ 0.0 × 10^6 J/m^3, which corresponds to the easy-plane anisotropy. The interface DMI constant D varies from 0.0 to 1.4 mJ/m^2, which is also typical for Co films on the heavy metal sublayer. The mesh element size 1.5 × 1.5 × 1.0 nm^3 is smaller than the exchange length.

A simple probe model in the form of uniformly magnetized Co sphere is used to simulate the effects of the interaction between the MFM probe and the film. The magnetic moment of the probe is

$$\mu = \frac{4\pi}{3} a^3 M_s \quad (1)$$

where M_S is the saturation magnetization of Co, $a = 20$ nm is the radius of sphere. This size is larger than the size of a superparamagnetic particle, we also assume the probe is coercive enough to keep it uniformly magnetized state.

The simulation of bimeron nucleation is done as follows. The starting point is the film uniformly magnetized along x-direction. Afterward we place MFM tip with magnetic moment oriented in z-direction at the height of 160 nm and apply homogeneous magnetic field of some magnitude controversial to the tip magnetic moment (Fig. 2). Then we simulate smooth movement of the MFM tip to the film from height of 160 nm to 20 nm with 20 nm step. The equilibrium magnetization distribution in the film is calculated at every step. Then we simulate smoother movement of the tip from 10 nm to 0 nm with 2 nm step. Two scenarios are possible depending on the influence of uniform external field magnitude. In the absence of external field or if the field is less than some critical value H_c a meron-antimeron pair is formed by the field of the tip (Fig. 2a) but annihilate when the tip moves away (see supplemental material). However if external field is higher than H_c the antimeron core is reversed along the field. So it also becomes a meron and the bimeron pair is formed (see supplemental material). The calculated H_c values are presented in Fig. 2e. They are in the range of 0.01 ÷ 0.20 T depending on the film material parameters. We do not found noticeable dependence of H_c on the D value, while it depends linearly on the anisotropy K_{eff} value. Since H_c is in the range of 0.01 ÷ 0.20 T it can be applied *in situ* without magnetic probe reversal[25,26]. If the values of K_{eff} and D correspond to the bimeron stability region (Fig. 2e), the bimeron stays stable after the tip is moved away and the uniform

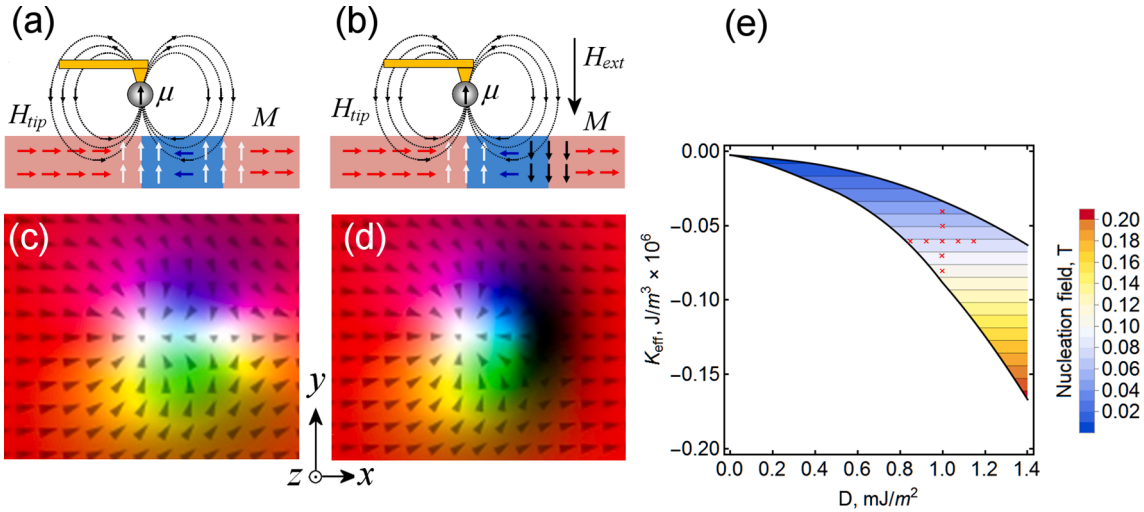

Fig. 2. (Color online) (a) Side view of the schematic distribution of the magnetic field H_{tip} created by the magnetic moment μ of the MFM probe and the magnetization M in the meron-antimeron pair arising in the magnetic film in this situation. (b) The same distributions when an additional external field is applied. One can see the magnetization reversal of the core of the antimeron and the emergence of a topologically charged meron pair - bimeron. (c) and (d) are the corresponding in-plane distributions of the magnetization. The size of the images corresponds to 218 × 178 nm^2. (e) The diagram indicating the region of bimeron stability. The color indicates the minimum value of the external magnetic field H_c required for the initialization of the bimeron. The crosses correspond to D and K_{eff} values for the calculated FMR spectra in (Fig. 4b,c).

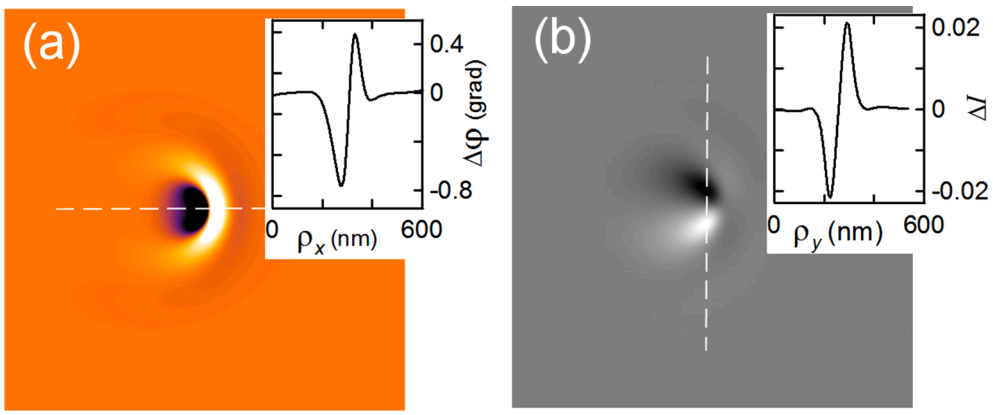

Fig. 3. (Color online). Calculated MFM (a) and LTEM (b) images of the bimeron. The insets demonstrate corresponding MFM and LTEM contrast profiles along the dashed lines. The size of the images is 768 × 768 nm^2.

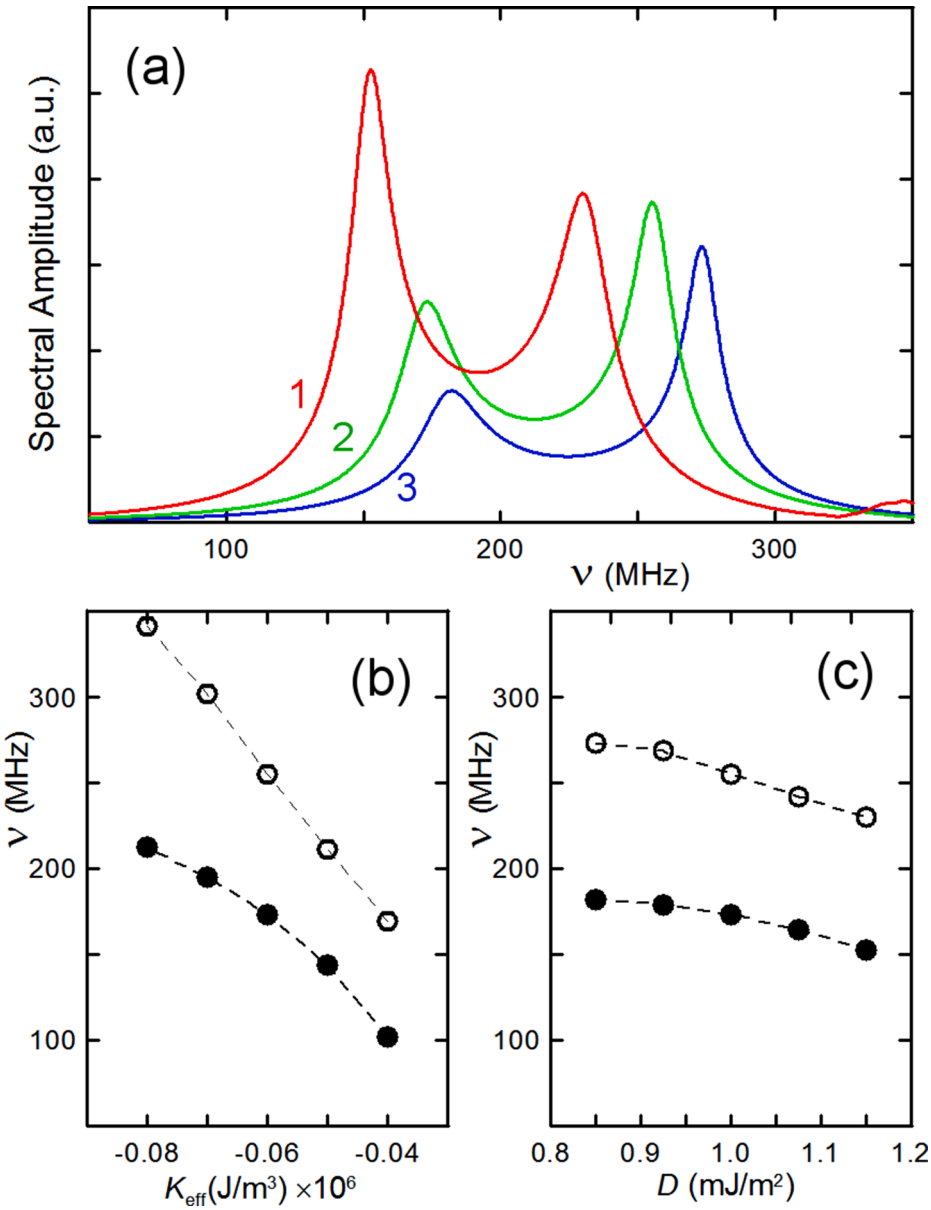

Fig. 4. (Color online) a) FMR spectra for magnetic bimeron in magnetic film with $K_{eff} = -0.06 \times 10^6$ J/m^3 and $D = 1.15$ mJ/m^2 (1, red line). $D = 1.00$ mJ/m^2 (2, green line) and $D = 0.85$ mJ/m^2 (3, blue line). The dependence of FMR frequencies on K_{eff} (b) and D (c) for the high frequency (open circles) and low frequency (filled circles) modes.

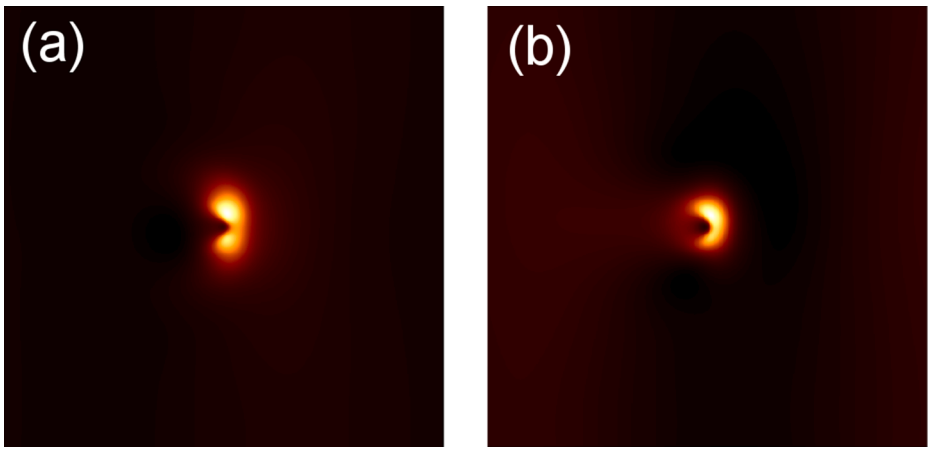

Fig. 5. (Color online). The normalized distributions of the oscillation amplitudes at the bimeron FMR (in arbitrary units): (a) low-frequency mode; (b) high-frequency mode. The size of the images is 768 × 768 nm^2.

external field is switched off. Moreover it stays stable if the initializing uniform external field is not switched off. This enables to successively nucleate a number of bimerons by the MFM tip touch in the different places of the same film.

To estimate the possibility of detecting the bimeron by conventional MFM and LTEM methods we calculate corresponding images (Fig. 3). For MFM we consider awidely used phase contrast imaging method. In this regime the MFM signal is registered as the phase shift $\Delta\varphi$ of cantilever oscillations under the magnetostatic interaction between tip and sample, which is[27,28]:

$$\Delta\varphi = -\frac{Q}{k}\frac{\partial F_z}{\partial z} \tag{2}$$

where Q is the cantilever quality factor, k is the cantilever force constant, and F_z is the z-component of magnetic force. In our calculations we use typical MFM probe parameters $Q = 100$ and $k = 6$ (N/m). The film-probe distance is 50 nm. In the point-dipole probe approximation, the force value is proportional to the second derivative of the sample magnetic stray field $\partial^2 H_z/\partial z^2$ at the point of the probe. It is calculated with the model magnetization distribution obtained from simulations (Fig. 1b). The calculated values $\Delta\varphi \sim 1$ (Fig. 3a) are typical for MFM measurements of magnetic skyrmions[29,30]. Thus, the localized bimeron can be detected by MFM methods.

A specially developed original Python script for the Gatan Microscopy Suite Software® 3.4.3 is used[31] to simulate LTEM images. The value of the Fresnel contrast ΔI is proportional to the projection of magnetization curl on the optical axis of an electron microscope $\boldsymbol{n}$ [32,33] and can be calculated as

$$\Delta I(\rho) = (n\cdot[\nabla \times M(r)]) \tag{3}$$

where $\boldsymbol{\rho}$ is a vector in the detector plane and $\boldsymbol{r}$ is a vector in the plane of the film. The calculated value ΔI=±0.02 is the same for numerically simulated skyrmion (Fig. 1a). So this contrast seems to be enough for bimeron detection[34]. Also recently, it have been reported about the experimental observation of domain wall bimerons by LTEM methods in thin CoZnMn films with easy-plane anisotropy[35]. (Domain wall bimeron is a topologically charged defect of a domain wall in a magnetic film).

MRFM is another very sensitive method to probe magnetic nanoobjects, which allows realizing FMR spectroscopy of magnetic nanostructures. We simulate the dynamics of the system using the ringdown method[36] to understand how bimeron changes FMR spectrum of the film. At the first stage, bimeron distribution is relaxed to the equilibrium state in the weak in-plane magnetic field ($\mu H = 5 \times 10^{-4}$ T). This field is necessary to remove degeneration of the bimeron energy according its orientation and to prevent the bimeron in-plane rotation during relaxation. Then a weak exciting field in the form of a rectangular pulse of 10^{-4} T amplitude and 0.4 ns duration is applied along x-axis (see geometry in Fig. 2d). Afterward the relaxation oscillations of the variable component of the magnetization are recorded for 800 ns (with 0.01 ns time resolution) and fast Fourier transform is performed to extract low-frequency resonant spectrum. The chosen orientation of the exciting field does not lead to oscillations in the uniformly magnetized film. The appearance of two resonances is observed in the low-frequency range of FMR spectra in the presence of the bimeron (Fig. 4a). These modes correspond to oscillations of the magnetization in the area of bimeron core.

The positions of the resonances depend both on anisotropy and DMI coefficient as it is presented on Fig. 4b,c. The corresponding values of the material parameters of the simulated system are denoted by crosses in Fig. 2e.

The typical distributions of amplitudes of resonant oscillations corresponding to these modes are presented in Fig. 5. The images are calculated for the film with $K_{eff} = -0.05 \times 10^6$ J/m^3 and D = 1.0 mJ/m^3 and demonstrate the value of

$$A(x,y) = < (M(x,y,t) - < M(x,y,t) >)^2 > \tag{4}$$

where $< >$ denotes the averaging over oscillation period. Evidently, the main power of oscillations is concentrated in the bimeron area. The amplitudes of these localized modes of resonance oscillations are high enough to detect them by MRFM[37,38].

Thus we performed the micromagnetic simulations of magnetic bimeron initialization by local magnetic field of magnetic force microscope probe in the in-plane magnetized thin Co film with interfacial Dzyaloshinskii-Moriya interaction. We demonstrate that the MFM probe approach accompanied by additional external magnetic field leads to the stable bimeron formation. The magnitude of required external field mainly depends on the parameter of magnetic anisotropy and is varied in the range of 0.01–0.20 mT. This is realized easily in commercial microscopes. In addition, we calculated the specific MFM and LTEM contrasts based on simulated bimeron magnetization distribution. Also we calculated the low-frequency FMR spectra indicating the appearance of two resonances connected with modes localized in the bimeron region. Performed calculations show that the individual bimeron can be detected by MFM, LTEM and MRFM methods.

CRediT authorship contribution statement

M.V. Sapozhnikov: Conceptualization, Methodology, Writing – original draft, Writing – review & editing, Investigation. **D.A. Tatarskiy:** Software, Writing – original draft, Visualization, Funding acquisition, Investigation. **V.L. Mironov:** Methodology, Writing – original draft,

Investigation.

Declaration of Competing Interest

The authors declare that they have no known competing financial interests or personal relationships that could have appeared to influence the work reported in this paper.

Acknowledgement

The authors are very grateful to A.A.Fraeman, A.G.Temiryazev and R.V. Gorev for useful discussions. This study is supported by the Russian Science Foundation (Grant no. 21-72-10176).

Appendix A. Supplementary material

Supplementary data to this article can be found online at https://doi.org/10.1016/j.jmmm.2022.169043.

References

[1] I.E. Dzyaloshinskii, B.A. Ivanov, JETP Lett. 29 (1979) 540.
[2] A.S. Kovalev, A.M. Kosevich, K.V. Maslov, JETP Lett. 30 (1979) 296.
[3] S. Muhlbauer, B. Binz, F. Jonietz, C. Pfleiderer, A. Rosch, A. Neubauer, R. Georgii, P. Boni, Sci. 323 (2009) 915.
[4] N. Bogdanov, Hubert, J. Magn. Magn. Mater. 138 (1994) 255.
[5] S. Heinze, K. von Bergmann, M. Menze, J. Brede, A. Kubetzka, R. Wiesendanger, G. Bihlmayer, S. Blugel, Nat. Phys. 7 (2011) 713.
[6] A. Fert, V. Cros, and Sampaio, Nat. Nanotechnol. 8 (2013) 152.
[7] X. Zhang, Y. Zhou, K.M. Song, T.-E. Park, J. Xia, M. Ezawa, X. Liu, W. Zhao, G. Zhao, S. Woo, J. Phys. Condens. Matter 32 (2020), 143001.
[8] H. Xia, C. Song, C. Jin, J. Wang, J. Wang, Q. Liu, J. Magnetism and Magnetic Materials 458 (2018) 57.
[9] Z. Li, Y. Zhang, Y. Huang, C. Wang, X. Zhang, Y. Liu, Y. Zhou, W. Kang, S.C. Koli, N. Lei, J. Magnetism and Magnetic Mat. 455 (2018) 19.
[10] J. Zang, M. Mostovoy, J.H. Han, N. Nagaosa, Phys. Rev. Lett. 107 (2011), 136804.
[11] B. Göbel, I. Mertig, O.A. Tretiakov, Phys. Reports 895 (2021) 1.
[12] Y.A. Kharkov, O.P. Sushkov, M. Mostovoy, Phys. Rev. Lett. 119 (2017), 207201.
[13] B. Göbel, A. Mook, J. Henk, I. Mertig, O.A. Tretiakov, Phys. Rev. B 99 (2019), 060407.
[14] O.G. Udalov, I.S. Beloborodov, M.V. Sapozhnikov, Phys. Rev. B 103 (2021), 174416.
[15] R. Zarzuela, V.K. Bharadwaj, K.-W. Kim, J. Sinova, K. Everschor-Sitte, Phys. Rev. B 101 (2020), 054405.
[16] X. Yu, W. Koshibae, Y. Tokunaga, K. Shibata, Y. Taguchi, N. Nagaosa, Y. Tokura, Nat. 564 (2018) 95.
[17] N. Gao, S.-G. Je, M.-Y. Im, J.W. Choi, M. Yang, Q.-C. Li, T. Wang, S. Lee, H.-S. Han, K.-S. Lee, W. Chao, C. Hwang, J. Li, Z.Q. Qiu, Nat. Commun. 10 (2019) 5603.
[18] J. Vijayakumar, Y. Li, D. Bracher, C.W. Barton, M. Horisberger, T.h. Thomson, J. Miles, C.h. Moutafis, Fr. Nolting, C.A.F. Vaz, Phys. Rev. Appl. 14 (2020), 054031.
[19] O.L. Ermolaeva, N.S. Gusev, E.V. Skorohodov, Y.V. Petrov, M.V. Sapozhnikov, V. L. Mironov, Mat. 10 (2017) 1034.
[20] A. Casiraghi, H. Corte-León, M. Vafaee, F. Garcia-Sanchez, G. Durin, M. Pasquale, G. Jakob, M. Kläui, O. Kazakova, Commun. Phys. 2 (2019) 145.
[21] A.V. Ognev, A.G. Kolesnikov, Y.J. Kim, I.H. Cha, A.V. Sadovnikov, S.A. Nikitov, I. V. Soldatov, A. Talapatra, J. Mohanty, M. Mruczkiewicz, Y. Ge, N. Kerber, F. Dittrich, P. Virnau, M. Kläui, Y.K. Kim, A.S. Samardak, ACS Nano 14 (2020) 14960.
[22] V.L. Mironov, A.A. Fraerman, O.L. Ermolaeva, Bulletin of the Russian Academy of Sciences: Physics 72 (2008) 1475.
[23] O. Klein, G. de Loubens, V.V. Naletov, F. Boust, T. Guillet, H. Hurdequint, A. Leksikov, A.N. Slavin, V.S. Tiberkevich, N. Vukadinovic, Phys. Rev. B 78 (2008), 144410.
[24] A. Vansteenkiste, J. Leliaert, M. Dvornik, M. Helsen, F. Garcia-Sanchez, B. Van Waeyenberge, AIP Adv. 4 (2014), 107133.
[25] N. Amos, R. Fernandez, R.M. Ikkawi, M. Shachar, Jeongmin Hong, Beomseop Lee, D. Litvinov, S. Khizroev, Ultrahigh coercivity magnetic force microscopy probes to analyze high moment magnetic structures and devices, IEEE Magnetic Letters 1 (2010) 6500104.
[26] O. Akdogan, N. G. Akdogan, SmCo-based MFM probes with high switching fields, J. Magnetism and Magnetic Materials 520 (2021) 167124, https://doi.org/10.1016/j.jmmm.2020.167124.
[27] D. Rugar, H.J. Mamin, P. Guethner, S.E. Lambert, J.E. Stern, I. McFadyen, T. Yogi, J. Appl. Phys. 68 (1990) 1169.
[28] A. Thiaville, J. Miltat, J.M. Garcia, Magnetic Force Microscopy: Images of Nanostructures and Contrast Modeling, in Magnetic Microscopy of Nanostructures, edited by H, in: Hopster and H.P, Oepen (Springer Verlag, Berlin, Heidelberg, 2005, p. 225.
[29] M.V. Sapozhnikov, Y.V. Petrov, N.S. Gusev, A.G. Temiryazev, O.L. Ermolaeva, V. L. Mironov, O.G. Udalov, Materials 13 (2020) 99.
[30] M.V. Sapozhnikov, N.S. Gusev, S.A. Gusev, D.A. Tatarskiy, Y.V. Petrov, A. G. Temiryazev, A.A. Fraerman, Phys. Rev. B 103 (2021), 054429.
[31] D. A. Tatarskiy "Fresnel contrast simulation for Gatan Microscopy Suite", https://doi.org/10.13140/RG.2.2.11313.40805.
[32] S. McVitie, G. White, J. Phys. D: Appl. Phys. 37 (2004) 280.
[33] S. McVitie, M. Cushley, Ultramicroscopy 106 (2006) 423.
[34] W. Jiang, S. Zhang, X. Wang, C. Phatak, Q. Wang, W. Zhang, M.B. Jungfleisch, J. E. Pearson, Y. Liu, J. Zang, X. Cheng, A. Petford-Long, A. Hoffmann, S.G.E. te Velthuis, Phys. Rev. B 99 (2019), 104402.
[35] T. Nagase, Y.-G. So, H. Yasui, T. Ishida, H.K. Yoshida, Y. Tanaka, K. Saitoh, N. Ikarashi, Y. Kawaguchi, M. Kuwahara, M. Nagao, Nat. Commun. 12 (2021) 3490.
[36] R.D. McMichael, M.D. Stiles, J. Appl. Phys. 97 (2005) 10J901.
[37] F. Guo, L.M. Belova, R.D. McMichael, Phys. Rev. Letters 110 (2013), 017601.
[38] A. Volodin, C. Van Haesendock, E.V. Skorokhodov, R.V. Gorev, V.L. Mironov, Appl. Phys. Lett. 113 (2018), 122407.